JOURNAL OF GEOPHYSICAL RESEARCH, VOL. 115, F02020, doi:10.1029/2009JF001314, 2010

An examination of seasonal deformation at the Portuguese Bend landslide, southern California, using radar interferometry

M. D. Calabro,[1] D. A. Schmidt,[1] and J. J. Roering[1]

Received 16 March 2009; revised 26 January 2010; accepted 3 February 2010; published 24 June 2010.

[1] The Portuguese Bend landslide, located on the Palos Verdes peninsula in southern California, is a slow-moving landslide whose activity is closely tied to infiltration from rainfall. We use radar interferometry to constrain the seasonal kinematics of the landslide from 1995 to 2000. Traditional interferometric synthetic aperture radar methods estimate an average downslope displacement rate of 1.00 m/yr with an uncertainty range of 0.39–2.57 m/yr during the summer months. Interferograms show a consistent loss in phase coherence over the landslide for epochs greater than 6 months, especially in the winter. Interferograms become incoherent as a result of large displacement, and decorrelation is used to map the spatial extent of slide movement through time. The displacement rate increases sharply several weeks after the beginning of the rainy season as rainwater percolating into the slide elevates pore pressures. Phase coherence is lost when the slide velocity surpasses ~2.6 m/yr for interferograms with durations of a few months. A physically based model based on rainfall-driven landslide movement incorporates these observations to constrain hydraulic diffusivity to between 0.9 and 3.5×10^{-6} m^2/yr.

Citation: Calabro, M. D., D. A. Schmidt, and J. J. Roering (2010), An examination of seasonal deformation at the Portuguese Bend landslide, southern California, using radar interferometry, *J. Geophys. Res.*, *115*, F02020, doi:10.1029/2009JF001314.

1. Introduction

[2] Landslides are the dominant mechanism of sediment production in mountainous terrain, and they can dam rivers, dictate the pace of bedrock channel incision, and incur substantial damage to infrastructure and/or human life. Given the diverse nature of triggering mechanisms (e.g., rainfall, earthquakes, frost cracking), documentation of landslide dynamics through monitoring is critical for evaluating hazard potential. Field-based monitoring of landslides can be both logistically challenging and costly. Recent advances in interferometric synthetic aperture radar (InSAR) have shown much potential in identifying and quantifying landslides [*Kimura and Yamaguchi*, 2000; *Ferretti et al.*, 2003; *Squarzoni et al.*, 2003; *Hilley et al.*, 2004; *Catani et al.*, 2005; *Finnegan et al.*, 2008]. These studies provide greater insight into the kinematics of active slides and help to constrain models of landslide dynamics. Of greatest concern are those landslides that are embedded in urban environments where slides pose a direct hazard to nearby structures [*Hilley et al.*, 2004].

[3] The Portuguese Bend landslide (PBL), which is surrounded by a coastal residential community in southern California, is one such slide that has received significant attention. The slide is located on the southwest coast of the Palos Verdes peninsula, 34 kilometers south of downtown Los Angeles (Figure 1). The PBL covers an area of 1.06 km^2, and it is part of a larger complex of landslides with an area of 6 km^2. In addition to the PBL, this complex includes the Abalone Cove landslide to the west, the Flying Triangle landslide to the northeast, and a large area of ancient inactive landslides to the north [*Ehlig*, 1992]. The earliest sliding on the Palos Verdes peninsula began upslope of the current active slide about 600,000 years ago [*Bryant*, 1982]. The majority of slides on this ancient complex, however, did not initiate until about 120,000 years ago, when high sea level eroded the area around Portuguese and Inspiration Points [*Ehlig*, 1986]. According to carbon-14 dating, the most recent ancient slides occurred around 4800 years ago, and were likely caused by the erosion of the toe of the Pleistocene slide [*Emery*, 1967].

[4] In 1956 the Portuguese Bend landslide was reactivated. Despite knowledge of the ancient slide [*Kew*, 1926; *Woodring et al.*, 1946], construction crews extending a road from the town of Rancho Palos Verdes dumped large amounts of fill to flatten the roadbed. In some areas they placed as much as 20 meters of fill, adding a significant load to the slope. Simultaneously, new housing developments in the area raised the water table through landscaping practices and newly installed septic systems [*Ehlig*, 1992]. Within months of the fill placement, the slide moved at a rate of several centimeters per day [*Vonder Linden*, 1989]. Since the initiation of the slide in 1956, deformation of the PBL has continued at rates varying with the seasons and rainfall levels. Between 1956 and 2002, the slide has traveled a total horizontal distance of 150–175 meters for an average displacement rate of 3.3–

[1]Department of Geological Sciences, University of Oregon, Eugene, Oregon, USA.

0148-0227/10/2009JF001314

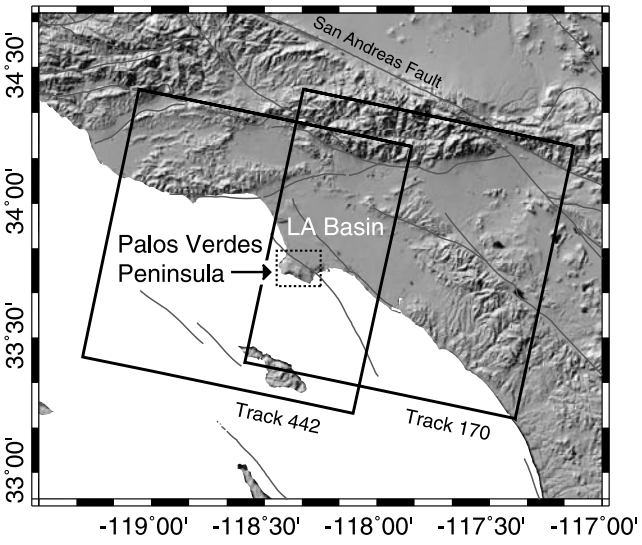

Figure 1. ERS satellite tracks (large boxes with solid black lines) covering the Palos Verdes peninsula. The Portuguese Bend landslide is on the southwest edge of the peninsula. The central box with a dotted black line indicates the region shown in Figure 2. Major faults are marked by dark gray lines [*Jennings*, 1994].

3.8 m/yr [*Kayen*, 2002]. Campaigns to dewater the landslide began in the 1980s, with limited success, reducing only the fastest sliding rates. The mid-1990s brought some of the highest rainfall levels recorded in the 121 year history of Los Angeles, including the El Niño event over the winter of 1997–1998. This increase in rainfall corresponded to an acceleration in displacement that slowed rapidly into the new millennium as rainfall levels subsided [*Kayen*, 2002].

[5] Despite an abundance of available satellite scenes, there has been no InSAR study of the PBL to date, perhaps due to the difficulty in observing the large magnitude surface displacements that are characteristic of the slide. In this study, some of the difficulties in quantifying the deformation are addressed, and ultimately the results are applied to the mechanics of the landslide.

1.1. Landslide Properties

[6] The bedrock underlying the Palos Verdes peninsula is composed primarily of Mesozoic Catalina Schist. The eastern section of the slide itself is underlain with Miocene sedimentary bedrock, while the western section is underlain by moderately stable ancient landslide deposits. The Monterey Formation overlays the schist, and is predominantly composed of Altamira Shale [*Vonder Linden*, 1989]. This shale is the primary rock type associated with the landslide. In addition, there are volcanic rocks and coastal deposits which were created concurrently with the shale. At the base of the landslide is a layer referred to as the Portuguese Tuff which has largely altered to bentonite due to chemical weathering [*Ehlig*, 1992].

[7] The Portuguese Bend is a hydrologically driven, slow-moving landslide complex with varying degrees of internal deformation [*Ehlig*, 1992]. Rainwater percolates through cracks, fissures and pore space in the slide, raising the water table and increasing pore pressures through the slide. The bottom of the slide is distinct and continuous, and is bound by the Portuguese Tuff aquiclude which precludes further downward flow [*Ehlig*, 1992]. The basic response of the slide can be understood using a landslide model first proposed by *Terzaghi* [1950], and recently quantified by *Iverson* [2000]. The failure surface of the slide has a bedding plane angle which varies from 22° at the head scarp to about 6° on the main portions of the slide [*Ehlig*, 1992]. The thickness of the slide varies from several meters to 75 meters, and averages about 18 meters [*Vonder Linden*, 1989]. As the modest success of the dewatering campaigns and rainfall driven acceleration suggest, the landslide depends greatly on groundwater and pore pressure [*Ehlig*, 1992]. Multiple studies [*Merriam*, 1960; *Vonder Linden*, 1989; *Ehlig*, 1992] agree that the displacement continues due to the constant coastal erosion at the toe of the slide.

1.2. Satellite Interferometry

[8] The primary observation method for this study is InSAR. Differential InSAR is most commonly used to measure deformation from active faulting and volcanic events, as well as aquifer subsidence (see references in the work by *Bürgmann et al.* [2000]). Less work has been done using InSAR to monitor landslides, as the large magnitude deformation rates associated with slides often makes conventional interferometry difficult or impossible. Most of the InSAR work on landslides has been done looking at mountainous slides [*Carnec et al.*, 1996; *Fruneau et al.*, 1996; *Squarzoni et al.*, 2003; *Colesanti et al.*, 2003; *Farina et al.*, 2006; *Catani et al.*, 2005]. Conventional InSAR studies have primarily used short-repeat cycle data, collected either during the ERS commissioning phase in 1991 (3 day repeat cycles), or on TANDEM missions in 1995, 1996, 1997 and 1999 (1 day repeat cycles) [*Carnec et al.*, 1996; *Fruneau et al.*, 1996; *Squarzoni et al.*, 2003]. *Kimura and Yamaguchi* [2000] examined a landslide in northern Japan using a multiple pass method with JERS L band (23.5 cm wavelength) data. The permanent scatterers method has been the most popular approach for dealing with the large displacements typical of landslides. Several studies [*Colesanti et al.*, 2003; *Ferretti et al.*, 2003; *Hilley et al.*, 2004; *Farina et al.*, 2006] have used permanent scatterers to successfully measure landslide displacement rates. Additionally, *Hilley et al.* [2004] relate sliding velocity in the Berkeley Hills of northern California to the lag time after the onset of the rainy season. Here we perform a similar analysis to estimate the hydraulic diffusivity at the PBL.

[9] No previous studies have examined the PBL using InSAR, possibly due to the large surface displacement at the site. The change in phase observed by the satellite cycles from 0 to 2π, and conventional InSAR requires that the change in phase from one pixel to the next is less than 2π radians, otherwise an ambiguity in the number of phase cycles exists [*Hanssen*, 2001]. One phase cycle of 2π corresponds to 2.8 cm of deformation along the satellite's line of sight (LOS) for C band satellites. In cases of very high strain, the observed phase change may cross this limit, becoming decorrelated over the deforming area [*Yun et al.*, 2007]. Rather than disregard those interferograms with decorrelated patches over the slide, they are used to constrain the spatial and temporal boundaries of the PBL by mapping the extent of

Table 1. ERS Interferograms Used to Make Summer Stacks

Starting Date	Ending Date
Track 170	
21 Apr 1995	26 May 1995
30 Jun 1995	8 Sep 1995
6 Apr 1996	28 Sep 1996
26 Apr 1997	31 May 1997
31 May 1997	5 Jul 1997
9 Aug 1997	13 Sep 1997
13 Sep 1997	18 Oct 1997
11 Apr 1998	25 Jul 1998
16 May 1998	20 Jun 1998
20 Jun 1998	3 Oct 1998
1 May 1999	23 Oct 1999
20 May 2000	2 Sep 2000
Track 442	
5 Apr 1995	14 Jun 1995
14 Jun 1995	19 Jul 1995
14 Jun 1995	23 Aug 1995
23 Aug 1995	27 Sep 1995
4 Jul 1996	17 Oct 1996
15 May 1997	19 Jun 1997
19 Jun 1997	24 Jul 1997
4 May 2000	8 Jun 2000

decorrelated phase. *Zebker et al.* [1996] utilize a similar technique to map decorrelation caused by terrain modification from active lava flows in Hawaii.

[10] InSAR processing has many benefits for measuring surface deformation. The displacement field obtained from InSAR is continuous with a pixel resolution of tens of meters. Additionally, InSAR yields LOS range change estimates with subcentimeter resolution. This data, however, is only one dimensional in nature, and must be modified to estimate the true displacement field. Since the satellite always observes the study area with the same viewing geometry, the three-dimensional displacement is projected on to the LOS vector from the satellite to the ground. Typically, data from ascending and descending tracks are used to approximate the 3-D displacement. However, ascending data is not available for the study area. Here, GPS data and topography are used to determine the orientation of the slide movement and convert the LOS observation to downslope movement.

2. Analysis of InSAR Data

[11] This study of the Portuguese Bend landslide uses data from the ERS satellite of the European Space Agency collected between 1992 and 2001. The Palos Verdes peninsula lies within the region overlapped by two paths of the satellite (tracks 170 and 442), effectively making available twice as many scenes over the region as is typical for InSAR studies. For each track, the area of interest is contained entirely within frame 2925 (Figure 1). For track 170, 19 scenes collected by ERS-1 and 57 by ERS-2 are used. Over track 442, 21 scenes collected by ERS-1 and 36 by ERS-2 are used. SAR data are first processed using the 2-pass method. The ROI PAC processing package is used to create differential interferograms from the raw ERS data [*Rosen et al.*, 2004]. A 1 arc sec (30 meter resolution) digital elevation model (DEM) collected during the Shuttle Radar Topography Mission (STRM) is used to remove the topographic component of the phase. All interferograms are processed at 4 looks in range. Only pairs of scenes with perpendicular baselines less than 200 meters are processed, totaling 288 interferograms along track 170, and 251 along track 442.

[12] Interferograms from both tracks contain decorrelated areas in the mountains and hills around the Los Angeles basin where steep topography reduces coherence. Interferograms maintain high coherence in the urban areas where buildings act as strong, stable reflectors. Within the frame we observe subsidence in previously studied basins [*Bawden et al.*, 2001; *Lanari et al.*, 2004] and deformation along the Newport-Inglewood fault which runs just north of the peninsula [*Watson et al.*, 2002].

[13] Many interferograms show a broad phase signal extending northwest to southeast along the length of the Palos Verdes peninsula. This broad phase signal is interpreted as an atmospheric artifact caused by water saturated air (such as fog) blowing off the ocean and hugging the ridge line. The same signal is identified by *Li et al.* [2005] and removed from their interferometric data set using MODIS atmospheric data. The high moisture content in the air column slows electromagnetic wave propagation in the atmosphere surrounding the ridge, resulting in a broad, distinct signal that is correlated to topography [*Hanssen et al.*, 1999]. To remove the signal, each interferogram is examined individually by plotting the phase of each pixel against the corresponding elevation from the DEM. After solving for the best linear fit through the scatter of points for each individual interferogram, the atmospheric component is estimated and removed from the phase. The PBL is small relative to the size of the peninsula and any downslope movement is not correlated with topography, so it remains unaffected by this correction. All interferograms in this study have had this atmospheric signal removed.

2.1. Summer Deformation

[14] Individual interferograms often do not show a definitive deformation signal over the landslide area because of a low signal-to-noise ratio for short-duration interferograms. Most of the interferograms are partially decorrelated over the sliding area, and interferograms that are coherent typically span a short time period (<105 days), typically in the summer months when velocities are slow. The lack of obvious deformation in the coherent interferograms is due to a low signal-to-noise ratio. The short temporal baseline and low sliding velocity in the summer months reduce the deformation observed in any single interferogram to near or below the magnitude of noise and other artifacts, such as from atmospheric effects.

[15] In order to better visualize the deformation in the study area, a stacking algorithm is employed to better isolate the deformation of the slide. 12 interferograms are stacked along track 170, and 8 interferograms are stacked along track 442 (Table 1). The data from each track must be stacked separately because of the difference in look angle across the scene. The interferograms selected for the stacks show good coherence over the slide, and interferograms with duplicate master or slave scenes are avoided so as to minimize any systematic biases. All Interferograms span less than 6 months between April and October of a given calendar year.

[16] The stacking of interferograms reveals deformation on the Palos Verdes peninsula that maps to the PBL. The average displacement rates of the landslide are 30.9 ±

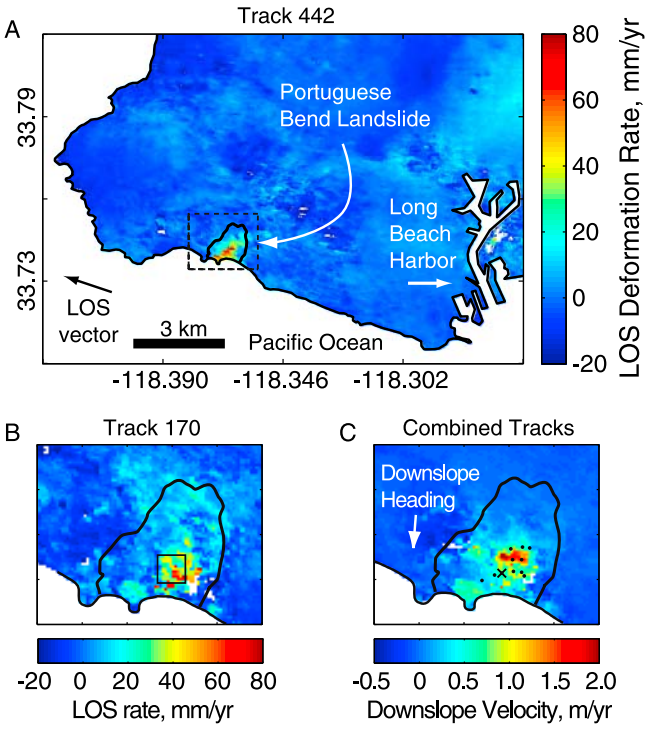

Figure 2. (a) A stack of 8 summer interferograms for track 442 of the ERS satellite between 1995 and 2000 on the Palos Verdes peninsula. The previously mapped maximum extent of the Portuguese Bend landslide is outlined in black. (b) The line-of-sight (LOS) rate is shown for a stack of 12 summer interferograms on track 170. The region shown corresponds to the dashed box in Figure 2a. The box outlined by a thin solid line highlights the area used for the averaging of the LOS rates reported in the text. (c) InSAR data from tracks 442 and 170 are back-projected onto a downslope unit vector to infer the average slide velocity in the summer. Dots are campaign GPS benchmarks used to determine an average surface velocity for comparison to InSAR. The cross marks the GPS station discussed in the text.

18.4 mm/yr for track 170 and 55.6 ± 17.9 mm/yr for track 442 along the satellite line of sight (Figure 2). The average is only taken over the area of the box shown in Figure 2b to avoid complications with uncertainties near the boundaries of the slide. Reported values are the mean sliding velocity plus or minus the standard deviation over the slide. The difference in displacement patterns between tracks 170 and 442 reflects different noise characteristics in the independent stacks, slightly different look angles, and different time sampling of a time-dependent signal. The high standard deviation is due to annual variations in the sliding rate, with some years exhibiting more deformation than others.

[17] The horizontal direction of deformation measured by campaign GPS along with the topographic slope inferred from a DEM is used to constrain the downslope displacement of the slide as observed by InSAR. The average horizontal bearing from GPS is 175.6° west of north, and this displacement direction is consistent with a downslope landslide mechanism. Because GPS is less reliable in the vertical direction than the horizontal [*Mao et al.*, 1999], the DEM is used to find the topographic slope that describes the vertical component of the unit displacement vector. The spatially variable slope is determined by taking a moving average of the gradient using a 750 m window. The smoothed DEM is used to account for the fact that the failure surface is likely smoother and more continuous than the surface topography. The values average 6.5° ± 0.9° with error due to variation across the slide, compared to a reported average dip of 6.3° for the failure surface by *Ehlig* [1992]. This defines a downslope unit vector for the slide of close to $(-0.990\hat{n}, -0.090\hat{e}, 0.110\hat{z})$. The corresponding unit look vector for the satellite is $(0.083\hat{n}, -0.332\hat{e}, \cos(\beta)\hat{z})$ where the vertical look angle β (~20°) depends on the position of the landslide within the frame. Projecting the downslope vector onto the look vector reveals that the satellite measurement is primarily sensitive to the vertical movement of the slide.

[18] Using the geometry of the satellite's unit look vector and the downslope unit vector of the PBL defined from GPS azimuth and DEM slope, we calculate the average downslope displacement rate for both tracks 170 and 442 (Figure 2c). For the pixels outlined by the box in Figure 2b, the average downslope velocity is found to be 1.00 m/yr. We assess the uncertainty of this back projection by using Monte Carlo sampling to propagate the uncertainties from the LOS observation and the look geometry. We determine the uncertainty in the LOS observation by adding in quadrature the standard deviation of the InSAR stack and the variation in rates across the region where the InSAR data are averaged (box in Figure 2b). We then estimate the uncertainty in the back projection by taking into account the uncertainty of the look vector assuming that the heading and look angle each vary by ±0.2° along the satellite's orbital path. For the downslope unit vector, we assume that the azimuth varies by ±2.7° and the surface slope can vary by ±0.9° across the slide. For each iteration, the variables used in the downslope calculation are resampled given their prescribed uncertainties. After performing 10^6 iterations, we find a lognormal distribution of downslope velocity that ranges between 0.39 to 2.57 m/yr (1-σ range about the mean of 1.00 m/yr).

[19] The city of Rancho Palos Verdes collected campaign GPS data starting in 1995 in order to monitor activity of the slide. Those data serve as a means to validate the previously described InSAR observations. Examining a single GPS site and InSAR pixel, we find similar results for the GPS and InSAR data during the period from 1995 and 2000. GPS site PB8 is marked with a cross in Figure 2c. This site was chosen because it is away from the edges of the slide and has a displacement direction close to average. The total GPS summer deformation rate at this site is 0.66 m/yr. No uncertainties were reported with the GPS data. The corresponding pixel for the stack of InSAR data on track 170 shows a downslope displacement rate of 0.68 ± 0.21 m/yr, while the same pixel on track 442 shows a downslope displacement rate of 0.87 ± 0.35 m/yr. The errors reported for these InSAR displacement rates are due to variations of individual interferograms within the stack. Over a broader region, the GPS sites indicated by black dots in Figure 2c show an average downslope deformation rate in the summer months of 1.17 ± 0.50 m/yr. The error reported is one standard deviation from the mean, representing the variability in results among the benchmarks.

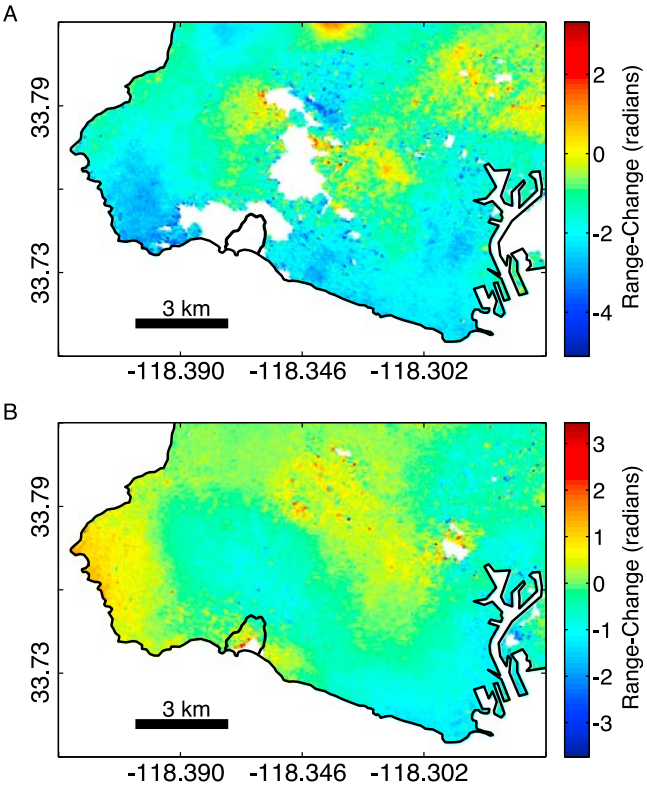

Figure 3. (a) A 385 day interferogram (16 May 1998 to 5 June 1999) shows large decorrelated patches over the vegetated regions of the peninsula. This is typical of interferograms longer than 1 year. The previously mapped maximum extent of the PBL is outlined in black. (b) A 35 day interferogram (23 December 1995 to 27 January 1996) shows decorrelated patches typical of winter interferograms. The area immediately over the landslide is decorrelated, while the surrounding area maintains phase coherence. The decorrelation in short-duration interferograms is likely caused by significant movement of the slide.

The GPS data from the summer months are consistent with the InSAR results (~1 m/yr) averaged over a similar region for the summers between 1995 and 2000.

[20] We also attempted to characterize the deformation using a persistent scatterer (PS) methodology. Using the StaMPS analysis package [*Hooper et al.*, 2007], several time series were created over the Palos Verdes peninsula. Although many scatterers were selected throughout the peninsula, none were selected on the landslide itself, so no estimation of displacement could be made. We suspect that PS InSAR was unsuccessful because the density of scatterers was too low within the slide and individual pixels could not unwrap due to the high and variable displacement rate.

2.2. Winter Deformation

[21] Most interferograms of the Palos Verdes peninsula that span winter months show pockets of decorrelation on and around the mapped area of the PBL. Decorrelated pixels identify areas where the complex radar echoes are not spatially coherent among neighboring surface scatterers. Decorrelation can be caused by a number of different processes, including instrument noise (i.e., thermal noise), changes in viewing geometry (baseline decorrelation), changes in surface properties (temporal decorrelation), steep topography, or difficulties with scene coregistration [*Zebker and Villasenor*, 1992; *Lee and Liu*, 2001].

[22] We attribute most of the decorrelation found in long-duration interferograms of the Palos Verdes peninsula to temporal decorrelation related to vegetation growth (Figure 3). Where not developed, the Palos Verdes peninsula is sparsely vegetated with coastal sage scrub and nonnative grass species [*Gabet and Dunne*, 2002]. The largest vegetated areas are on the southwest coast of the peninsula, including the PBL and surrounding areas. The city has placed development restrictions on this land because of current and recent landsliding and evidence of ancient landslides. Interferograms with durations greater than 1 year show broad regions of decorrelated phase that closely match the vegetated regions on the peninsula, and thus the decorrelation is likely due to the cumulative effects of vegetation growth.

[23] The major cause of decorrelation for short-duration interferograms over the PBL is an unwrapping failure due to the steep deformation gradient along the edge of the landslide. Since the boundary zone where the slide ramps from zero deformation to a fast sliding rate is small, the shear strain is quite large (~0.05 strain). Decorrelation can result if the spatial gradient in the phase is too high and the fringe pattern is lost [*Yun et al.*, 2007]. In addition to the loss in signal along the margins of the slide, internal deformation within the slide likely contributes to the decorrelation in the interior. The lack of decorrelation in similarly vegetated areas around the PBL rules out vegetation as the main cause of decorrelation over the PBL for interferograms that span less than 1 year. The decorrelated patches are typically confined within the boundaries of the mapped landslide and do not extend into the surrounding areas (Figure 3b). The surrounding areas maintain a coherent phase signal for timescales of less than 1 year, after which they become decorrelated as well.

[24] The mapping of decorrelated phase yields information on both the spatial and temporal characteristics of the PBL. A similar application of the phase decorrelation was used by *Zebker et al.* [1996] to map the extent of active lava flows. Decorrelation is dependent on both the phase coherence and choice of multilooking, and can be inferred from the variance of the phase [*Rodriguez and Martin*, 1992]. For this analysis, a given pixel is considered decorrelated if the standard deviation of the filtered phase exceeds 1 radian within a 5 × 5 pixel window. The extent of the landslide can be determined by mapping the decorrelated phase through time. For each day of the year, the decorrelation level, I, is the ratio of the number of interferograms in which a given pixel is decorrelated to the number of total interferograms that span that day. This ratio is calculated as

$$I_{i,t} = \frac{n_{i,t}}{N_{i,t}}, \tag{1}$$

where i is the pixel index, n is the number of decorrelated interferograms, N is the total number of interferograms that span a particular day t. A decorrelation level of 0.8 means that 80% of the interferograms are decorrelated on that day for that pixel. To minimize any bias from vegetation growth, all

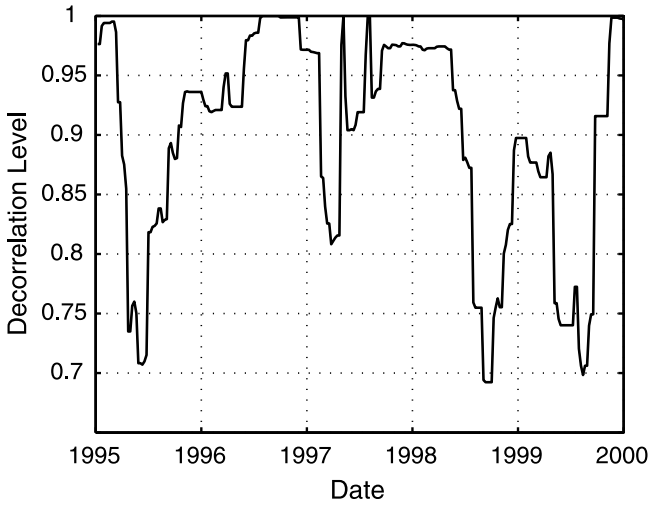

Figure 4. Full time series of average decorrelation level over the mapped landslide. The decorrelation level does not fall as expected during the summer of 1996 due to the lack of short-duration summer interferograms and high rainfall during the spring. The El Niño year of 1997–1998 exhibits increased decorrelation level through the spring.

interferograms with durations greater than 12 months are excluded. The spatial average of the decorrelation level over all pixels in the mapped landslide is plotted in a time series from 1995 to 2000 using 157 interferograms (Figure 4). In this set, there are about the same number of short-, intermediate-, and long-duration interferograms (all between 35 days and 1 year), and they are roughly distributed equally throughout the year to eliminate potential biases. This plot shows a substantial decrease in I during the summers of 1995, 1998, and 1999 when the slide slows and short-duration interferograms regain phase coherence. The decorrelation extends longer into the spring of 1998 than other years. This delay is attributed to the El Niño winter of 1997–1998 which prolonged the high sliding rate into the late spring.

[25] The results for the summers of 1996 and 1997 highlight the problems encountered by plotting the full time series. The temporal resolution for this method is low, and it misses trends that occur over a short time span. Because new SAR scenes are acquired at most twice every 35 days (once for track 170 and once for track 442), there are often too few interferograms that span a specific day and I becomes quantized. For instance, if a date is spanned by only three interferograms, the possible decorrelation levels are 0, 1/3, 2/3 and 1. A decrease in decorrelation level during the summer of 1996 is obscured by the lack of short-duration interferograms that summer. The nominal value for I is high (generally >0.7) because yearlong interferograms contain both the winter and summer seasons. High decorrelation in the winter biases the decorrelation level toward higher levels.

[26] Stacking all of the data onto a 1 year time frame increases temporal resolution, revealing the spatial evolution through the winter season. This method collapses all 5 years of data onto a single calendar year, which effectively yields a multiyear average for the decorrelation over the landslide (Figure 5). With this technique, decorrelation is mapped as a function of space and time. As the slide accelerates through the late fall and into the winter months, the decorrelation level increases first in the center of the slide and migrates outward. This trend then reverses going into the spring and summer. Because the decorrelation level is averaged over several years using interferograms with various temporal and perpendicular baselines, the result is a qualitative measure of landslide activity. The value of the decorrelation level cannot be used as a direct proxy for sliding velocity. Rather, relative shifts in its level are indicative of when the phase gradient passes a critical threshold. When the decorrelation level ramps up sharply, it is a sign that the phase gradient threshold has been crossed. And when it drops, coherence has recovered and the slide has slowed enough to allow for successful unwrapping of the phase.

2.3. Kinematic Constraints From Decorrelation

[27] The decorrelation mapping gives information on the spatial and temporal extent of the PBL. Specifically, the analysis shows that the phase becomes decorrelated over the landslide at the end of each fall as the slide begins to accelerate. Here we attempt to quantify the downslope velocity when decorrelation occurs. The maximum theoretical phase gradient for successful phase unwrapping corresponds to one fringe per pixel [*Massonnet and Feigl*, 1998]. However the phase gradient threshold is expected to decrease as multiple factors act to lower the coherence level of the radar echoes. *Baran et al.* [2005] explored the dependence of the phase gradient threshold on coherence, and developed an empirical relationship.

[28] We determine the maximum detectable phase gradient for our data set by using a similar empirical approach as *Baran et al.* [2005]. The phase gradient threshold is determined by taking 5 interferograms of the study area, each with different durations (35–105 days) and perpendicular baselines (37–127 m). A bell-shaped deformation signal is added to the multilooked wrapped interferogram. The processing then proceeds as normal ending with an unwrapped georeferenced differential interferogram (Figure 6a). By using the actual interferograms over the Palos Verdes peninsula, the inherent noise characteristics of the data are preserved, and the processing procedures (such as filtering) are consistent with those used to process the rest of the InSAR data set. After converting the phase from radians to meters and using a pixel dimension of 30 meters, we find that decorrelation occurs when the phase gradient exceeds a threshold of $\sim 1.4 \times 10^{-4}$ (Figure 6b). This threshold can vary within the range of $1–2 \times 10^{-4}$ depending on the duration of the interferogram, the perpendicular baseline, topography, as well as other factors. Our threshold is consistent with that found by *Baran et al.* [2005] for coherence levels of ~0.37.

[29] The phase gradient threshold is then used to constrain the LOS rate when decorrelation occurs. For this calculation the landslide is assumed to be described by a block where strain is concentrated along the margins. The actual deformation gradient around the PBL varies significantly along the margins of the slide. The west side of the slide ramps up to high deformation over a very short distant (within meters), while the east side of the slide changes much more gradually (within 100 meters) [*Ehlig*, 1992]. An average boundary width of about two pixels (~60 meters) is used in this study. Thus for the shortest possible epoch (35 days), and the width

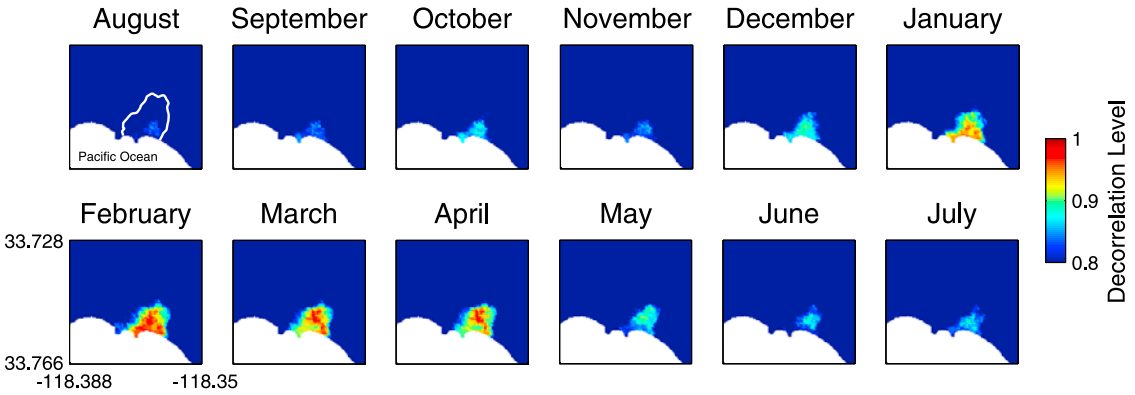

Figure 5. The spatial and temporal variation in the decorrelation level at the Portuguese Bend landslide. Several years of data (1995–2000) are condensed onto a single calendar year and binned by month. Blue areas have low levels of decorrelation. Warm-colored areas are decorrelated for nearly every interferogram for a given month due to high rates of sliding. The decorrelation increases sharply in December and decreases in May, consistent with the seasonal acceleration of the slide. The white line in the first frame shows the mapped extent of the landslide.

of 60 meters for the margin of the slide, the maximum observable deformation rate is 13 cm/yr along the satellite LOS, with an uncertainty range of 9–19 cm/yr given the range in the phase gradient threshold. The LOS rate from a summer stack of interferograms (~5 cm/yr) is well below this value, as expected. This LOS rate of 13 cm/yr corresponds to a downslope displacement rate of 2.6 m/yr, with an uncertainty range of 1.9–3.7 m/yr.

[30] Since the sharp change in decorrelation corresponds to the time when the maximum detectable phase gradient is exceeded, decorrelation mapping can constrain the time when a pixel exceeds the velocity threshold. Figure 7 shows the decorrelation level over the slide based on all interferograms with epochs less than 1 year, condensed into a single calendar year. A sharp increase in decorrelation occurs within the month of December. Similarly, a sharp decrease in decorrelation occurs within the month of May, so the downslope velocity drops back below ~2.6 m/yr.

2.4. Rainfall and Slide Activity

[31] Previous work shows that the Portuguese Bend landslide is hydrologically driven, with the sliding velocity increasing as the water table rises and pore pressure increases [*Ehlig*, 1992]. As pore pressure diffuses through the slide there is a lag between the onset of rainfall and the acceleration of the slide. Rain gauge data collected by the city of Palos Verdes can be combined with the decorrelation level to measure how long it takes after the rainy season begins for the slide to cross the phase gradient threshold.

[32] It is important to note that one does not expect a direct relationship between the amplitudes of rainfall and decorrelation. Decorrelation does not measure the deformation rate of the slide directly, and once the slide becomes decorrelated the sliding velocity can continue to increase with no change in the decorrelation level. Only the sharp changes in the decorrelation level are noteworthy.

[33] Rain gauge data are analyzed to determine when the rainy season begins. The water year begins 1 October each year, while precipitation is still at the extremely low summer level (Figure 7). A cumulative rainfall amount of 1.9 cm is used as a threshold to mark the onset of the rainy season. Only trace amounts of rain fall each water year before crossing this threshold, and once cumulative rainfall exceeds 1.9 cm, it tends to continue raining consistently. While it would be preferred to compare a full time series of the decorrelation level to the rainfall from 1995 to 2000, the temporal resolution of the decorrelation level is too low to retrieve lag times on a yearly basis. Averaging rain gauge data from October 1995 to October 1999 yields a rainfall initiation date of 15 November, plus or minus two weeks. With the increased decorrelation over the slide confined to the month of December, the lag time between the onset of rainfall and the acceleration of the slide to velocities ≥2.6 m/yr is about 1 month. It is also possible that the slide could respond to individual storms during the winter season. However, we would be unable to resolve this given the temporal sampling of the InSAR data.

3. Modeling for Hydraulic Diffusivity

[34] *Iverson*'s [2000] model predicts a relationship between landslide velocity and time lag following a rainfall event and describes how pore pressure diffuses through a landslide on different timescales. Here the model is evaluated as one potential application of the results obtained from the InSAR data. Both the Minor Creek and the Portuguese Bend landslides are hydrologically driven and slow moving, allowing a valid comparison between the two systems. *Iverson* [2000] derives the following equation based on his dynamic model:

$$\frac{dv^*}{dt^*} = S\sin\alpha[1 - FS_0(Z)] + S\frac{\gamma_w}{\gamma_s}\frac{\tan\phi}{\cos\alpha}\frac{I_z}{K_z} \cdot \begin{cases} [R(t^*)] & t^* \le T^* \\ [R(t^*) - R(t^* - T^*)] & t^* > T^*. \end{cases} \quad (2)$$

[35] On the left-hand side is the derivative of the normalized velocity, v^*, with respect to normalized time, t^*. The

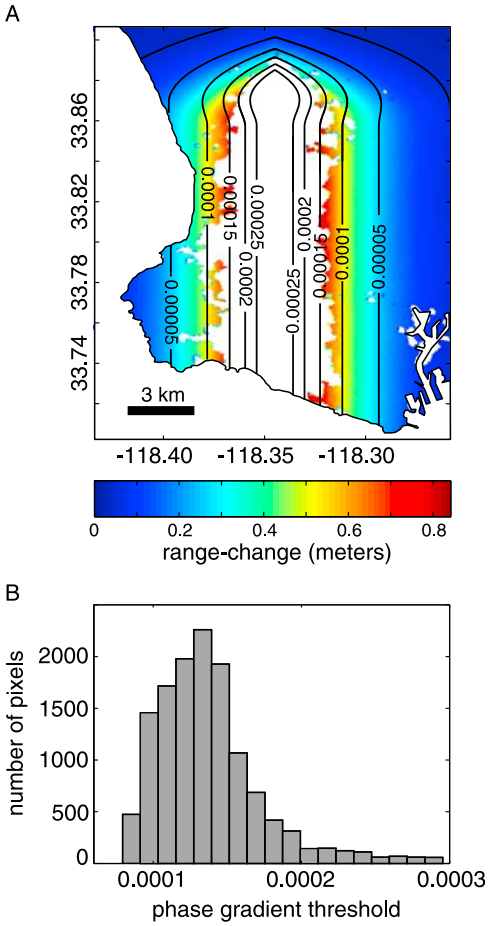

Figure 6. (a) The maximum phase gradient above which the phase becomes decorrelated is evaluated by adding a deformation signal to an interferogram (15 May 1997 to 19 June 1997) over the Palos Verdes peninsula. The interior white region is decorrelated because of a steep phase gradient (black contours calculated from the input deformation signal). (b) A histogram of the maximum phase gradient threshold inferred from 5 interferograms. The phase is decorrelated for phase gradients greater than ~1.4×10^{-4}.

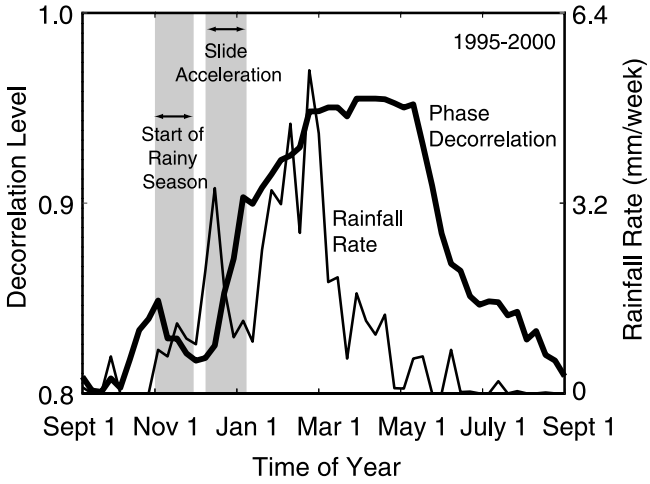

Figure 7. The average decorrelation level on the PBL (bold line) is compared to the average rainfall rate on the Palos Verdes peninsula (thin line). Data from 1995 to 2000 are stacked onto a 1 year period. The gray vertical bars indicate the onset of rainfall in November and the initiation of fast deformation rates in December. The lag between the two is about 1 month. The start of the rainy season is defined here as when the cumulative rainfall reaches 1.9 cm. The acceleration of the slide is indicated by a rapid increase in the decorrelation level.

velocity has been normalized so that $v^* = v/\sqrt{Zg}$, where Z is the depth of the slide and g is gravity. On the right-hand side of equation (2) are two terms. The first includes the factor of safety (FS), which is set to 1 for the point at which slope failure occurs. The remainder of the equation is a function of the normalized time, t^*, where $t^* = (4D_o t \cos 2\alpha)/Z^2$. The diffusivity, D_o, is the variable that will ultimately be estimated in our analysis. The other coefficients are properties of the landslide: γ_s is soil unit weight, γ_w is pore water unit weight, α is slope angle, ϕ is friction angle, S is a scaling coefficient, and I_z/K_z is the infiltration rate normalized by the vertical hydraulic conductivity. The normalized time, t^*, appears in the form of Richard's equation, as shown below:

$$R(t^*) = \sqrt{t^*/\pi}\exp(-1/t^*) - \mathrm{erfc}\left(1/\sqrt{t^*}\right). \qquad (3)$$

[36] *Iverson* [2000] uses known parameters from Minor Creek to predict the landslide velocity. The decorrelation analysis yields the landslide velocity at one specific time from the onset of rainfall. Fitting the model to the velocity data, an estimate for D_o, can be achieved. Here we assume that pore pressure variations on the PBL evolve according to a vertically oriented Darcy flow, rather than fracture-dominated transport, which may generate much more rapid response times. Diffusivity plays a vital role in slide mechanics because it dictates how quickly fluctuations in pore pressures propagate through the slide. The unknown parameters in equation (2) are the normalized vertical infiltration rate, I_z/K_z, and the diffusivity, D_o. Because the modeled velocity is much more sensitive to diffusivity than infiltration rate, we constrain D_o for the full range of realistic values of I_z/K_z [*Iverson*, 2000]. Additional parameter values are listed in Table 2.

[37] Integrating equation (2) yields the velocity, v^*, with respect to the time since rainfall onset, t^*. The two open circles in Figure 8a are the summer displacement rate from the InSAR stack and the winter displacement rate constrained by the maximum detectable phase gradient. Reasonable values of I_z/K_z are between 0.1 and 5, so the vertical infiltration rate is between one tenth and five times the vertical hydraulic conductivity. For a given D_o, varying I_z/K_z between 0.1 and 5 creates a family of curves whose extremes bound the shaded areas in Figure 8. The value of D_o

Table 2. Modeling Parameters for the PBL

Parameter	Variable	Value
Slope angle	α	6.3°
Landslide depth	Z	18 m
Friction angle	ϕ	6°
Soil unit weight, wet	γ_s	22,000 N/m^3

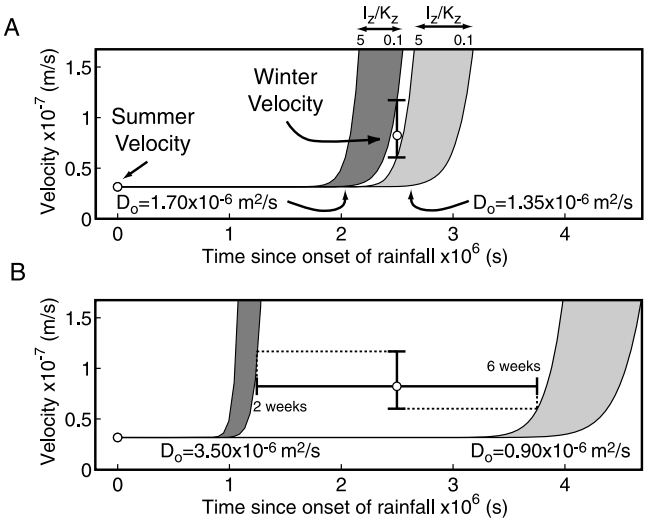

Figure 8. Modeling results for slide velocity as a function of time since the onset of rainfall. Open circles mark the summer and winter velocity constrained by InSAR. The sliding velocity is used to constrain the hydraulic diffusivity D_o using the model of *Iverson* [2000]. The normalized infiltration rate I_z/K_z is allowed to vary over a wide range. (a) The winter velocity occurs 4 weeks following the onset of the rainy season. The dark gray shaded region uses $D_o = 1.70 \times 10^{-6}$ m^2/s, and the light gray shaded region uses $D_o = 1.35 \times 10^{-6}$ m^2/s, given the uncertainty in the winter velocity. Within each shaded region, I_z/K_z ranges from 0.1 (right end) to 5.0 (left end) of each region. (b) The sensitivity of the model is analyzed accounting for the uncertainty in the lag time since the onset of rainfall (2–6 weeks). The diffusivity is constrained between 3.5×10^{-6} m^2/s and 0.9×10^{-6} m^2/s for the same range of I_z/K_z as in Figure 8a.

that fits for the most extreme case of I_z/K_z is used to constrain D_o. Higher values of I_z/K_z push the curve to the left, lower values push it to the right. In Figure 8a, the lower family of curves (light gray region) corresponds to $D_o = 1.35 \times 10^{-6}$ m^2/s, and higher family of curves (dark gray region) to $D_o = 1.70 \times 10^{-6}$ m^2/s. Even with a loose constraint on I_z/K_z, the model constrains D_o to a relatively narrow band of values.

[38] The time lag between onset of rainfall and fast displacement rate corresponding to the maximum detectable phase gradient is only a rough estimate. In addition to setting the lag to four weeks, D_o is also found given 50% error in this value, allowing the lag time to range from two to six weeks (Figure 8b). I_z/K_z is still allowed to vary through all reasonable values. This method now puts the outer bounds for diffusivity at 0.9×10^{-6} m^2/s and 3.5×10^{-6} m^2/s. *Iverson* [2000] finds $D_o = 1 \times 10^{-6}$ m^2/s at the Minor Creek landslide, similar to the value found for the PBL.

[39] *Hilley et al.* [2004] report a lag time between the beginning of the rainy season and the sharp increase in sliding velocity at the Berkeley Hills of up to ~3 months. At Minor Creek, *Iverson* [2000] finds a lag time of 5–8 days. Through InSAR observations, the lag time at the PBL is estimated to be 2–6 weeks. These three landslides are hydrologically similar, each characterized by slow, noncatastrophic movement. However, they have very different responses to rainfall. Examining the landslide parameters, landslide depth may be a dominant factor in this response. A deeper landslide should have a more delayed response to rainfall if the diffusivities are the same. The depth of the Minor Creek landslide is about 6 meters and it has the shortest lag time [*Iverson*, 2000]. While the average depth at the PBL is 18 meters [*Vonder Linden*, 1989], and it has an intermediate lag time. The Berkeley Hills slides have the longest lag time and the greatest depth, at about 30 meters [*Hilley et al.*, 2004].

4. Summary and Conclusion

[40] This study of the Portuguese Bend landslide has incorporated several different remote sensing methods in an attempt to monitor the slide, better understand its seasonal dynamics, and constrain physical parameters. The mean summer deformation rate of 1.00 m/yr with 1-sigma uncertainty range of 0.39 to 2.57 m/yr falls within one standard deviation of the summer rate measured by campaign GPS (1.17 ± 0.50 m/yr). While individual several month long to yearlong interferograms are not necessarily coherent over the landslide, enough short-time span interferograms during the summer months are coherent to obtain an average deformation rate for the same time period. This result is encouraging in that many short-duration interferograms can be stacked to reveal a landslide signal.

[41] Although phase decorrelation is often ignored in InSAR studies, it actually yields important information about the PBL. By mapping decorrelation through time, the spatial boundaries of the landslide are estimated and agree with the boundaries mapped in the field. Additionally, the timing of when the slide accelerates to velocities greater than 2.6 m/yr, as characterized by the steep phase gradient along the edges of the slide, is confined between the months of December and May. Combining this result with rain gauge data, the lag time between the onset of rainfall and the acceleration of the slide is determined to be about 1 month. Mapping phase decorrelation requires a larger data set than the stacking techniques used for coherent summer interferograms. If enough scenes are collected, this method can be used to track the evolution of events (such as landslides) where the deformation rate is otherwise too fast.

[42] The increased decorrelation level in the winter demonstrates that the landslide moves faster in the winter than the summer, consistent with previous studies that suggest that the slide is hydrologically driven. During the summer months the water table drops, reducing the pore pressure at the base of the slide, increasing frictional resistance, and decreasing slide velocity in response. Once rainfall reinitiates in the fall, there is about a 2–6 week lag time during which the rainwater generates pore pressure waves that percolate down through the slide, reducing frictional resistance and increasing sliding velocity.

[43] Applying the *Iverson* [2000] landslide model to the PBL, we constrain the hydraulic diffusivity to be between 0.9×10^{-6} and 3.5×10^{-6} m^2/s, despite significant uncertainty in the lag time. This diffusivity is similar to or slightly higher than that of the Minor Creek landslide, which *Iverson and Major* [1987] examine in detail. Comparing physical parameters at the PBL to those determined at Minor Creek

[*Iverson*, 2000] and the Berkeley Hills [*Hilley et al.*, 2004], the PBL is found to have both an intermediate lag time and landslide depth. The lag time is 2–6 weeks, as compared to 5–8 days at Minor Creek and ~3 months at the Berkeley hills, and the landslide depth is 18 meters, compared to 6 meters at Minor Creek and 30 meters at the Berkeley Hills. This suggests that for landslides with similar hydrologic properties, depth is an important factor in determining the slide's response to rainfall.

[44] **Acknowledgments.** We thank Robert Douglas for sharing the campaign GPS solutions for the Palos Verdes peninsula. Computational resources were funded by NSF (EAR-0651123).

References

Baran, I., M. Stewart, and S. Claessens (2005), A new functional model for determining minimum and maximum detectable deformation gradient resolved by satellite radar interferometry, *IEEE Trans. Geosci. Remote Sens.*, *43*, 675–682.

Bawden, G. W., W. Thatcher, and R. S. Stein (2001), Tectonic contraction across Los Angeles after removal of groundwater pumping effects, *Nature*, *412*(6849), 812–815.

Bryant, M. E. (1982), Geomorphology, neotectonics, and ages of marine terraces, Palos Verdes peninsula, in *Landslides and Landslide Mitigation in Southern California*, edited by J. D. Cooper, pp. 15–25, Assoc. of Eng. Geol., South. Calif. Section, Glendale.

Bürgmann, R., P. A. Rosen, and E. J. Fielding (2000), Synthetic aperture radar interferometry to measure Earth's surface topography and its deformation, *Ann. Rev. Earth Planet. Sci.*, *28*, 169–209.

Carnec, C., D. Massonnet, and C. King (1996), Two examples of the use of SAR interferometry on displacement fields of small spatial extent, *Geophys. Res. Lett.*, *23*, 3579–3582.

Catani, F., P. Farina, S. Moretti, G. Nico, and T. Strozzi (2005), On the application of SAR interferometry to geomorphological studies: Estimation of landform attributes and mass movements, *Geomorphology*, *66*, 119–131.

Colesanti, C., A. Ferretti, C. Prati, and F. Rocca (2003), Monitoring landslides and tectonic motions with the permanent scatterers technique, *Eng. Geol.*, *68*, 3–14.

Ehlig, P. L. (1986), The Portuguese Bend landslide: Its mechanics and a plan for its stabilization, in *Landslides and Landslide Mitigation in Southern California: Guidebook and Volume—Prepared for the 82nd Annual Meeting of the Cordilleran Section of the Geological Society of America*, edited by P. L. Ehlig, pp. 167–172, Geol. Soc. of Am., Boulder, Colo.

Ehlig, P. L. (1992), *Evolution, Mechanics and Mitigation of the Portuguese Bend Landslide, Palos Verdes Peninsula, California*, *Spec. Publ.*, vol. 4, pp. 531–553, Assoc. of Eng. Geol., Denver, Colo.

Emery, K. O. (1967), The activity of coastal landslides related to sea level, *Rev. Geogr. Phys. Geol. Dyn.*, *9*, 177–180.

Farina, P., D. Colombo, A. Fumagalli, F. Marks, and S. Moretti (2006), Permanent scatterers for landslide investigations: Outcomes from the ERS-SLAM project, *Eng. Geol.*, *88*, 200–217.

Ferretti, A., A. Prati, F. Rocca, N. Casagli, P. Farina, and B. Young (2003), Permanent scatterers technology: A powerful state of the art tool for historic and future monitoring of landslides and other terrain instability phenomena, in *Proceedings of 2005 International Conference on Landslide Risk Management* [CD-ROM], A. A. Balkerna, Vancouver, B. C., Canada.

Finnegan, N. J., M. E. Pritchard, R. B. Lohman, and P. R. Lundgren (2008), Constraints on surface deformation in the Seattle, WA, urban corridor from satellite radar interferometry time-series analysis, *Geophys. J. Int.*, *174*, 29–41.

Fruneau, B., J. Achache, and C. Delacourt (1996), Observation and modeling of the Saint-Étienne-de-Tinée landslide using SAR interferometry, *Tectonophysics*, *265*, 181–190.

Gabet, E. J., and T. Dunne (2002), Landslides on coastal sage-scrub and grassland hillslopes in a severe El Niño winter: The effects of vegetation conversion on sediment delivery, *Geol. Soc. Am. Bull.*, *114*, 983–990.

Hanssen, R. F. (2001), *Radar Interferometry: Data Interpretation and Error Analysis*, Springer, New York.

Hanssen, R. F., T. M. Weckwerth, H. A. Zebker and R. Klees (1999), High-resolution water vapor mapping from interferometric radar measurements, *Science*, *283*, 1297–1299.

Hilley, G. E., R. Bürgmann, A. Ferretti, F. Novali, and F. Rocca (2004), Dynamics of slow-moving landslides from permanent scatterer analysis, *Science*, *304*, 1952–1955.

Hooper, A., P. Segall, and H. Zebker (2007), Persistent scatterer interferometric synthetic aperture radar for crustal deformation analysis, with application to Volcán Alcedo, Galápagos, *J. Geophys. Res.*, *112*, B07407, doi:10.1029/2006JB004763.

Iverson, R. M. (2000), Landslide triggering by rain infiltration, *Water Resour. Res.*, *36*, 1897–1910.

Iverson, R. M., and J. J. Major (1987), Rainfall, ground-water flow, and seasonal movement at Minor Creek landslide, northwestern California: Physical interpretation of empirical relations, *Geol. Soc. Am. Bull.*, *99*, 579–594.

Jennings, C. W. (1994), Fault activity map of California and adjacent areas, *Geol. Data Map 6*, scale 1:750,000, Calif. Div. of Mines and Geol., Sacramento.

Kayen, R. E. (2002), Influence of the Portuguese Bend landslide on the character of the effluent-affected sediment deposit, Palos Verdes margin, southern California, *Cont. Shelf Res.*, *22*, 911–922.

Kew, W. S. (1926), Geologic and physiographic features in the San Pedro Hills, Los Angeles County, California, *Oil Bull.*, *12*, 513–518.

Kimura, H., and Y. Yamaguchi (2000), Detection of landslide areas using satellite radar interferometry, *Photogramm. Eng. Remote Sens.*, *66*, 337–344.

Lanari, R., P. Lundgren, M. Manzo, and F. Casu (2004), Satellite radar interferometry time series analysis of surface deformation for Los Angeles, California, *Geophys. Res. Lett.*, *31*, L23613, doi:10.1029/2004GL021294.

Lee, H., and J. G. Liu (2001), Analysis of topographic decorrelation in SAR interferometry using ratio coherence imagery, *IEEE Trans. Geosci. Remote Sens.*, *39*, 223–232.

Li, Z., J.-P. Muller, P. Cross, and E. J. Fielding (2005), Interferometric synthetic aperture radar (InSAR) atmospheric correction: GPS, Moderate Resolution Imaging Spectroradiometer (MODIS), and InSAR integration, *J. Geophys. Res.*, *110*, B03410, doi:10.1029/2004JB003446.

Mao, A., C. G. A. Harrison, and T. H. Dixon (1999), Noise in GPS coordinate time series, *J. Geophys. Res.*, *104*, 2797–2816.

Massonnet, D., and K. L. Feigl (1998), Radar interferometry and its application to changes in the Earth's surface, *Rev. Geophys.*, *36*, 441–500.

Merriam, R. (1960), Portuguese Bend landslide, Pales Verdes Hills, California, *J. Geol.*, *68*, 140–153.

Rodriguez, E., and J. M. Martin (1992), Theory and design of interferometric synthetic aperture radars, *IEE Proc., Part F*, *139*(2), 147–159.

Rosen, P. A., S. Hensley, G. Peltzer, and M. Simons (2004), Updated repeat orbit interferometry package released, *Eos Trans. AGU*, *85*(5), 47, doi:10.1029/2004EO050004.

Squarzoni, C., C. Delacourt, and P. Allemand (2003), Nine years of spatial and temporal evolution of the La Valette landslide observed by SAR interferometry, *Eng. Geol.*, *68*, 53–66.

Terzaghi, K. (1950), Mechanics of landslides, in *Application of Geology to Engineering Practice*, edited by S. Paige, pp. 83–123, Geol. Soc. of Am., Berkeley, Calif.

Vonder Linden, K. (1989), The Portuguese Bend landslide, *Eng. Geol.*, *27*, 301–373.

Watson, K. M., Y. Bock, and D. T. Sandwell (2002), Satellite interferometric observations of displacements associated with seasonal groundwater in the Los Angeles basin, *J. Geophys. Res.*, *107*(B4), 2074, doi:10.1029/2001JB000470.

Woodring, W. P., M. N. Bramlette, and W. S. W. Kew (1946), *Geology and Paleontology of the Palos Verdes Hills, California*, *U.S. Geol. Surv. Prof. Pap.*, *207*, 145 pp.

Yun, S.-H., H. Zebker, P. Segall, A. Hooper, and M. Poland (2007), Interferogram formation in the presence of complex and large deformation, *Geophys. Res. Lett.*, *34*, L12305, doi:10.1029/2007GL029745.

Zebker, H. A., and J. Villasenor (1992), Decorrelation in interferometric radar echoes, *IEEE Trans. Geosci. Remote Sens.*, *30*, 950–959.

Zebker, H. A., P. A. Rosen, S. Hensley, and P. Mouginis-Mark (1996), Analysis of active lava flows on Kilauea Volcano, Hawaii, using SIR-C radar correlation measurements, *Geology*, *24*, 495–498.

M. D. Calabro, J. J. Roering, and D. A. Schmidt, Department of Geological Sciences, 1272 University of Oregon, Eugene, OR 97403, USA. (mdcalabro@gmail.com; das@uoregon.edu)